

Automated Neutrino Jet and Top Jet Predictions at Next-to-Leading-Order with Parton Shower Matching in Effective Left-Right Symmetric Models

Olivier Mattelaer,^{1,*} Manimala Mitra,^{2,†} and Richard Ruiz^{3,‡}

¹*Centre for Cosmology, Particle Physics and Phenomenology (CP3),
Université catholique de Louvain, B-1348 Louvain-la-Neuve, Belgium*

²*Department of Physics, Indian Institute of Science Education and Research Mohali (IISER Mohali),
Sector 81, SAS Nagar, Manauli 140306, India*

³*Institute for Particle Physics Phenomenology (IPPP),
Department of Physics, Durham University, Durham, DH1 3LE, UK*

(Dated: October 31, 2016)

Hadronic decays of boosted resonances, e.g., top quark jets, at hadronic super colliders are frequent predictions in TeV-scale extensions of the Standard Model of Particle Physics. In such scenarios, accurate modeling of QCD radiation is necessary for trustworthy predictions. We present the automation of fully differential, next-to-leading-order (NLO) in QCD corrections with parton shower (PS) matching for an effective Left-Right Symmetric Model (LRSM) that features W_R^\pm, Z_R gauge bosons and heavy Majorana neutrinos N . Publicly available universal model files require remarkably fewer user inputs for predicting benchmark collider processes than leading order LRSM constructions. We present predictions for inclusive W_R^\pm, Z_R production at the $\sqrt{s} = 13$ TeV Large Hadron Collider (LHC) and a hypothetical future 100 TeV Very Large Hadron Collider (VLHC), as well as inclusive N production for a hypothetical Large Hadron Electron Collider (LHeC). As a case study, we investigate at NLO+PS accuracy the properties of heavy neutrino (color-singlet) jets and top quark (color-triplet) jets from decays of high-mass W_R bosons at the LHC. Contrary to top jets, we find that the kinematic properties of heavy neutrinos jets, and in particular jet mass, are resilient against the effects of parton showers and hard QCD radiation. This suggests that in searches for neutrino jets, aggressive selection cuts that would otherwise be inappropriate for top jets can be imposed with minimal signal loss.

Keywords: Automation, NLO Computations, Neutrinos Mass Models, Boosted Topologies

* olivier.mattelaer@uclouvain.be

† manimala@iisermohali.ac.in

‡ richard.ruiz@durham.ac.uk

CONTENTS

I.	Introduction	2
II.	Effective Left-Right Symmetric Model	4
	A. Collider Constraints on Effective LRSM	7
	B. Limitations of the Effective Left-Right Symmetric Model	7
III.	Computational Setup and Signal Modeling	8
	A. Model Implementation	8
	B. Monte Carlo Configuration	8
	C. Spin-Correlated Decays of N and t with Improved MadSpin	9
IV.	Results	10
	A. Inclusive W_R, Z_R Production in Hadron-Hadron Collisions	10
	B. Inclusive N Production in Hadron-Electron Collisions	12
	C. Kinematics of Neutrino and Top Jets at NLO+PS in LHC Collisions	14
V.	Summary and Conclusion	19
	Acknowledgments	20
	A. EffLRSM@NLO Signal Simulation with MG5_aMC@NLO	20
	B. Three-Body Decays of N and t in MadSpin	21
	C. User Defined Generator-Level Cuts in MG5_aMC@NLO	22
	References	23

I. INTRODUCTION

The Left Right Symmetric Model (LRSM) [1–3] is an economic and well-defined solution to a number of discrepancies within the Standard Model of particle physics (SM). Such issues include: the origin and lightness of neutrino masses, the existence of dark matter, and the baryon-antibaryon asymmetry of the universe. The model, based on the gauge group

$$SU(3)_c \otimes SU(2)_L \otimes SU(2)_R \otimes U(1)_{B-L}, \quad (1)$$

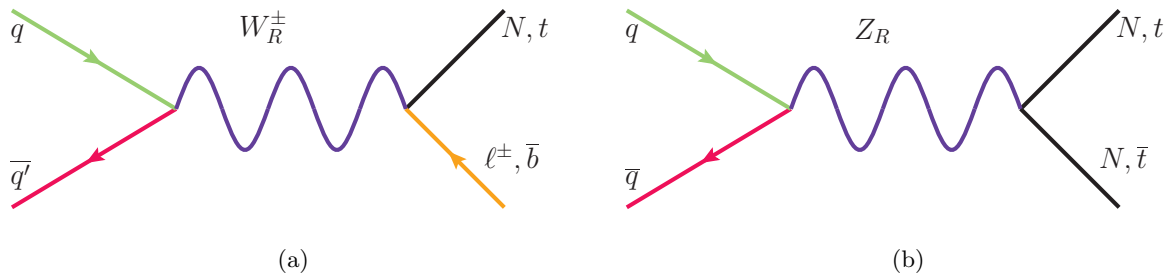


FIG. 1. Feynman diagrams of Born-level N and t production through (a) W_R and (b) Z_R in hadron collisions. All figures drawn with JaxoDraw [4].

predicts right-handed (RH) currents and the existence of heavy, RH gauge bosons W_R^\pm and Z_R . In addition, the model contains three RH neutrinos N_R that are charged under $SU(2)_R \otimes U(1)_{B-L}$ but singlets under SM symmetries. For masses up to several TeV, the LRSM can be tested at collider experiments such as the Large Hadron Collider (LHC) through searches for processes like

$$p p \rightarrow W_R^\pm \rightarrow t\bar{b} \text{ or } N_R \ell^\pm, \quad \text{with } N_R \rightarrow \ell^\pm W_R^{\mp*} \rightarrow \ell^\pm q \bar{q}', \quad \text{and} \quad (2)$$

$$p p \rightarrow Z_R \rightarrow t\bar{t} \text{ or } N_R N_R, \quad \text{with } \ell \in \{e, \mu, \tau\}, \quad q \in \{u, c, d, s, t, b\}, \quad (3)$$

and are shown diagrammatically in Fig. 1. The channels lead to the distinct $\ell^\pm \ell^\pm + nj$ [5], $\ell^\pm + j$ [6, 7], and single top [8] topologies, and have been studied extensively [6–21].

Monte Carlo (MC) modeling of the above processes by LHC experiments typically [22–25] involve leading order (LO) simulations matched to parton showers (PS) and are normalized with constant factors, so-called K -factors, to account for QCD corrections. While sufficient for predicting total inclusive cross sections, the procedure does not correctly capture the kinematic changes induced by high-transverse momentum (p_T) initial-state radiation (ISR) or final-state radiation (FSR). This can substantially impact experimental sensitivity, particularly as W_R (Z_R) decays to top quarks involve up to four (six) energetic jets at LO. Jet matching schemes at a scale $\mu \ll M_{V_R}$, for $V_R = W_R, Z_R$, can alleviate such problems. However, missing virtual corrections give rise to potentially unstable soft/collinear logarithms of the form $\alpha_s(M_{V_R}^2) \log(M_{V_R}^2/\mu^2)$ that spoil perturbative convergence for sufficiently large (M_{V_R}/μ) ratios. Furthermore, decays of high-mass RH gauge bosons to top quarks and heavy neutrinos can give rise to top [26–28] and heavy neutrino [7] jets, which carry different color charges, and hence possess different QCD radiation patterns. Observables sensitive to the structure of these jets, e.g., jet mass, can be used to discriminate against SM backgrounds but require information that first arises with $\mathcal{O}(\alpha_s)$ corrections.

To resolve these complications, we present the automation of next-to-leading-order (NLO) in

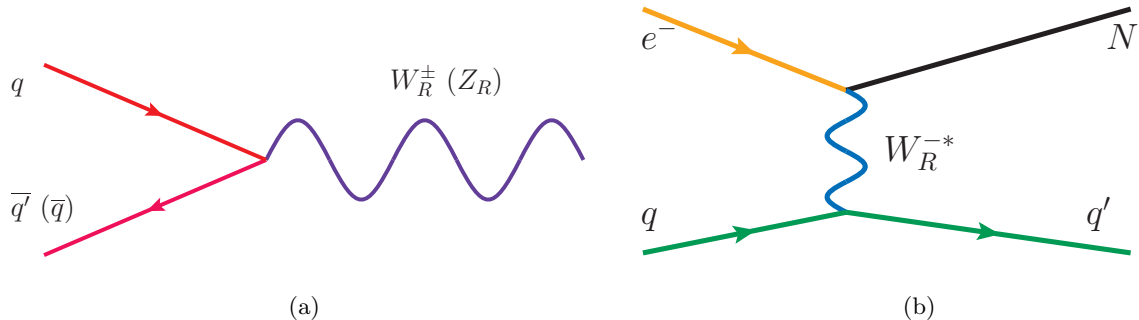


FIG. 2. Born-level (a) W_R, Z_R production in hadron collisions and (b) N production in ep collisions.

QCD corrections with parton shower (PS) matching for an effective LRSM, using the FeynRules (FR) + NLOCT + MadGraph5_aMC@NLO (MG5_aMC@NLO) [29–32] framework. The universal FR object (UFO) files [33] are publicly available from [34] and require remarkably fewer inputs for simulating fully differential, benchmark collider processes than current LO implementations [35–37]. We demonstrate this by providing predictions for W_R, Z_R production at the $\sqrt{s} = 13$ TeV LHC and a future 100 TeV Very Large Hadron Collider (VLHC) [38]. We also present predictions for inclusive N production at a hypothetical Large Hadron Electron Collider (LHeC) [39]. The Born diagrams for these processes are shown in Fig. 2. As a case study, we investigate at NLO+PS accuracy the properties of heavy neutrino (color-singlet) jets and top quark (color-triplet) jets from decays of high-mass W_R bosons at the LHC.

The remainder of the study proceeds in following manner: In Sec. II, we describe our effective LRSM model, and our computation setup in Sec. III. We present our results in Sec. IV, and then summarize and conclude in Sec. V. Instructions for using the EffLRSM@NLO model file within MG5_aMC@NLO are briefly provided in Apps. A-C.

II. EFFECTIVE LEFT-RIGHT SYMMETRIC MODEL

The Effective LRSM field content consists of the usual SM states, the W_R^\pm and Z_R gauge bosons, which are aligned with their mass eigenstates, and three heavy Majorana neutrinos N_i , aligned with the RH chiral states.

In the LRSM, the W_R chiral coupling to quarks are given by

$$\mathcal{L}_{W_R-q-q'} = \frac{-\kappa_R^q g}{\sqrt{2}} \sum_{i,j=u,d,\dots} \bar{u}_i V_{ij}^{\text{CKM}'} W_{R\mu}^+ \gamma^\mu P_R d_j + \text{H.c.}, \quad (4)$$

Here, $u_i(d_j)$ is an up-(down-)type quark of flavor $i(j)$; $P_{R(L)} = \frac{1}{2}(1 \pm \gamma^5)$ denotes the RH(LH)

Gauge Group	Charge	u_L	d_L	ν_L	e_L	u_R	d_R	N_R	e_R
$SU(2)_L$	$T_L^{3,f}$	$+\frac{1}{2}$	$-\frac{1}{2}$	$+\frac{1}{2}$	$-\frac{1}{2}$	0	0	0	0
$SU(2)_R$	$T_R^{3,f}$	0	0	0	0	$+\frac{1}{2}$	$-\frac{1}{2}$	$+\frac{1}{2}$	$-\frac{1}{2}$
$U(1)_{EM}$	Q^f	$+\frac{2}{3}$	$-\frac{1}{3}$	0	-1	$+\frac{2}{3}$	$-\frac{1}{3}$	0	-1

TABLE I. $SU(2)_L$, $SU(2)_R$, and $U(1)_{EM}$ quantum number assignments for chiral fermions f in LRSM.

chiral projection operator; and $V_{ij}^{CKM'}$ is the RH Cabbibo-Kobayashi-Masakawa (CKM) matrix, which is related to the SM CKM matrix. Throughout this study, we will assume five massless quarks and take both the SM and RH CKM matrices to be diagonal with unit entries. $g = \sqrt{4\pi\alpha_{EM}(M_Z)}/\sin\theta_W$ is the SM Weak coupling constant and $\kappa_R^q \in \mathbb{R}$ is an overall normalization for the W_R interaction strength.

For leptons, the W_R coupling and leptonic mixing is parametrized by [12, 40]

$$\mathcal{L}_{W_R-\ell-\nu/N} = \frac{-\kappa_R^\ell g}{\sqrt{2}} \sum_{\ell=e,\mu,\tau} \left[\sum_{m=1}^3 \bar{\nu}_m^c X_{\ell m} + \sum_{m'=1}^3 \overline{N_{m'}} Y_{\ell m'} \right] W_{R\mu}^+ \gamma^\mu P_R \ell^- + \text{H.c.} \quad (5)$$

The matrix $Y_{\ell m'}(X_{\ell m})$ quantifies the mixing between the heavy (light) neutrino mass eigenstate $N_{m'}$ (ν_m) and the RH chiral state with corresponding lepton flavor ℓ . The mixing scale as [5]

$$|Y_{\ell m'}|^2 \sim \mathcal{O}(1) \quad \text{and} \quad |X_{\ell m}|^2 \sim 1 - |Y_{\ell m'}|^2 \sim \mathcal{O}(m_{\nu_m}/m_{N_{m'}}). \quad (6)$$

As in the quark sector, $\kappa_R^\ell \in \mathbb{R}$ independently normalizes the W_R coupling strength to leptons. At TeV collider scales, both light neutrino masses and light neutrino mixing can be taken to zero. So for simplicity, we take $Y_{\ell m'}$ to be diagonal with unit entries:

$$|Y_{eN}| = |Y_{\mu N_2}| = |Y_{\tau N_3}| = 1, \quad |Y_{\text{others}}| = |X_{\ell m}| = 0. \quad (7)$$

Mass and mixing assumptions are modifiable in the public model files [34] but requires UFO regeneration. Specifically, do not load the FR restrictions, “massless.rst” and “diagonalCKM.rst”.

After LR symmetry breaking, the W_R^3 and $X_{(B-L)}$ gauge states mix and give rise to the massive Z_R and massless (hypercharge) B bosons. Subsequently, all fermions with $(B-L)$ charges, including ν_L and N_R , couple to Z_R . For chiral fermion f , we parametrize the Z_R neutral currents by

$$\mathcal{L}_{Z_R-f-f} = \frac{-\kappa_R^f g}{\sqrt{1 - (1/\kappa_R^f)^2 \tan^2 \theta_W}} \sum_{f=u,e,\dots} \bar{f} Z_{R\mu} \gamma^\mu \left(g_L^{Z_R,f} P_L + g_R^{Z_R,f} P_R \right) f. \quad (8)$$

	Mass [GeV]	$t\bar{b}$	$\ell^+ N_1$	$q\bar{q}'/q\bar{q}$	$t\bar{t}$	$\ell^+ \ell^-$	$\nu_e \nu_e$	$N_1 N_1$	Total
$\Gamma(W_R^+ \rightarrow X)$ [GeV]	3000	25.2	8.41	50.7	84.3
$\Gamma(Z_R \rightarrow X)$ [GeV]	5070	82.3	11.3	7.64	2.78	10.2	114
$\Gamma(N_1 \rightarrow e^\pm q\bar{q}')$ [GeV]	173.3	2.12×10^{-8}

TABLE II. Masses and total widths of W_R , Z_R and N_1 for representative parameters in Eq.(19).

κ_R^f are the same $\kappa_R^{q,\ell}$ as for W_R . In terms of electric and isospin charges, the chiral coefficients are

$$g_L^{Z_R,f} = \left(T_L^{3,f} - Q^f \right) \frac{1}{\kappa_R^f} \tan^2 \theta_W, \quad (9)$$

$$g_R^{Z_R,f} = T_R^{3,f} - \frac{1}{\kappa_R^f} \tan^2 \theta_W Q^f. \quad (10)$$

$SU(2)_L$, $SU(2)_R$, and $U(1)_{EM}$ quantum number assignments for f are summarize in Tbl. I.

For generic $\kappa_R^{q,\ell}$ normalizations, the LO W_R, Z_R partial decay widths are then

$$\Gamma(W_R \rightarrow q\bar{q}') = N_c |V_{qq'}^{CKM'}|^2 \frac{\kappa_R^{q2} g^2 M_{W_R}}{48\pi} \quad (11)$$

$$\Gamma(W_R \rightarrow t\bar{b}) = N_c |V_{tb}^{CKM'}|^2 \frac{\kappa_R^{q2} g^2 M_{W_R}}{48\pi} \left(1 - r_t^{W_R}\right)^2 \left(1 + \frac{1}{2} r_t^{W_R}\right), \quad (12)$$

$$\Gamma(W_R \rightarrow \ell N_{m'}) = |Y_{\ell N_{m'}}|^2 \frac{\kappa_R^{\ell 2} g^2 M_{W_R}}{48\pi} \left(1 - r_N^{W_R}\right)^2 \left(1 + \frac{1}{2} r_N^{W_R}\right), \quad (13)$$

$$\Gamma(Z_R \rightarrow f\bar{f}) = N_c^f \frac{\kappa_{Z_R}^{f2} g^2 M_{Z_R} \sqrt{1 - 4r_f^{Z_R}}}{48\pi \left[1 - (1/\kappa_R^f)^2 \tan^2 \theta_W\right]} \times \left[(g_L^{Z_R,f} + g_R^{Z_R,f})^2 (1 + 2r_f^{Z_R}) + (g_L^{Z_R,f} - g_R^{Z_R,f})^2 (1 - 4r_f^{Z_R}) \right] \quad (14)$$

$$r_i^{Z_R} = \frac{m_i^2}{M_{Z_R}^2}. \quad (15)$$

Assuming diagonal quark mixing and lepton mixing in Eq. (7), the total W_R, Z_R widths are then

$$\Gamma_{W_R} = 2\Gamma(W_R \rightarrow q\bar{q}') + \Gamma(W_R \rightarrow t\bar{b}) + \Gamma(W_R \rightarrow e N_1) + \Gamma(W_R \rightarrow \mu N_2) + \Gamma(W_R \rightarrow \tau N_3) \quad (16)$$

$$\Gamma_{Z_R} = \sum_f \Gamma(Z_R \rightarrow f\bar{f}) \quad (17)$$

While we take M_{W_R} and M_{Z_R} as independent phenomenological parameters, they are related in the LRSM by the relation

$$M_{Z_R} = \sqrt{2 \cos^2 \theta_W / \cos 2\theta_W} \times M_{W_R} \approx (1.7) \times M_{W_R} \quad (18)$$

As the size of $m_{N_{m'}}$ are governed by Yukawa couplings, the masses of $N_{m'}$ are largely independent of M_{W_R} . For the following representative input,

$$M_{W_R} = 3 \text{ TeV}, \quad m_{N_1} = m_t = 173.3 \text{ GeV}, \quad \text{and} \quad m_{N_2}, m_{N_3} = 10^{12} \text{ GeV}, \quad (19)$$

which we will motivate in the next section, the corresponding partial and total widths for W_R, Z_R , and N_1 are summarized in Tb. II. We have checked our model against these analytic results.

A. Collider Constraints on Effective LRSM

Direct and indirect tests place stringent limits on the LRSM. For a recent review, see [7] and references therein. Current LHC dijet and dileptons+jets searches require [22–25]:

$$M_{W_R} > 2.6 - 2.7 \text{ TeV} \quad \text{at} \quad 95\% \quad \text{CL} \quad \text{for} \quad \kappa_R^{q,\ell} = 1. \quad (20)$$

Using the $M_{W_R} - M_{Z_R}$ mass relation of Eq. (18), the subsequently limit on M_{Z_R} is:

$$M_{Z_R} > 4.4 - 4.6 \text{ TeV} \quad \text{at} \quad 95\% \quad \text{CL} \quad \text{for} \quad \kappa_R^{q,\ell} = 1. \quad (21)$$

Heavy neutrino masses remain unconstrained at colliders for $(m_{N_{m'}}/M_{W_R}) \lesssim 0.1$ due a breakdown of standard collider searches [7]. We exploit this latitude and equate the lightest heavy neutrino mass, which we denote for simplicity as N with mass m_N , to the top quark mass, m_t . For simplicity, we decouple the two remaining heavy neutrinos with unrealistically large masses. We do not advocate such a scenario will be realized in nature. This mass assignment permits us to make a more systematic comparison of heavy neutrino and top jets in Sec. IV C. We summarize our choices of LRSM inputs in Eq. (19).

B. Limitations of the Effective Left-Right Symmetric Model

The Effective LRSM is sufficient to describe at NLO+PS accuracy resonant production and decay of W_R, Z_R , and N in $pp/ep/ee$ collisions, and in particular the processes listed in Eqs. (2)-(3). This is done with minimal couplings, as seen in Eqs. (4)-(8). A limitation of the model is that it does not extend the SM Higgs sector to include the LRSM scalar fields. Constraints from flavor changing neutral current processes imply that the LRSM Higgs masses are as heavy as 15-20 TeV, and hence decouple from LHC phenomenology [7, 41–44]. It is this exclusion that gives the Effective LRSM its flexibility. However, as a consequence, non-Abelian W_R and Z_R interactions, as well as their couplings to SM bosons, are ill-defined. Phenomenologically, this implies that

most resonant pair production and vector boson scattering processes involving W_R and Z_R are not correctly modeled. The SM, on the other hand, is fully supported.

III. COMPUTATIONAL SETUP AND SIGNAL MODELING

A. Model Implementation

We implement the SM Lagrangian with Goldstone boson couplings in the Feynman gauge and the Lagrangian terms of Eqs. (4)-(8) in the Unitary gauge into FR 2.3.10 [29, 30]. R_2 rational and QCD renormalization counter terms are calculated with NLOCT 1.02 [31] and FeynArts 3.8 [45]. UFO model files are publicly available from the FR model database [34], and can be ported into modern event generators, including MG5_aMC@NLO [32], HERWIG [46], and SHERPA [47].

B. Monte Carlo Configuration

Fully differential results at LO and NLO are obtained using MG5_aMC@NLO 2.5.β2 [32]. Events are parton showered and hadronized using Pythia 8.219 (PY8) [48], and passed to MadAnalysis5 v1.4 [49] for particle-level clustering. Unless stated otherwise, jets are clustered via FastJet 3.2.1 [50, 51] according to the anti- k_T algorithm [52] with a separation scale of $R = 0.4$.

LRSM inputs are given in Eq. (19). SM inputs are taken from the 2014 Particle Data Group [53]:

$$\alpha^{\overline{\text{MS}}}(M_Z) = 1/127.940, \quad M_Z = 91.1876 \text{ GeV}, \quad \sin^2_{\overline{\text{MS}}}(\theta_W) = 0.23126. \quad (22)$$

We use the NLO NNPDF3.0 parton distribution function (PDF) set (1had=260000) [54] for LO and NLO calculations. PDFs and $\alpha_s(\mu_r)$ are extracted using LHAPDF 6.1.6 [55]. For all processes, we equate the renormalization (μ_r) and factorization (μ_f) scales. We choose as a dynamical scale, half the sum over all final-state transverse energies:

$$\mu_r, \mu_f = \mu_0 \equiv \sum_{k=N,\ell,\text{jets}} \frac{E_{T,k}}{2} = \frac{1}{2} \sum_k \sqrt{m_k^2 + p_{T,k}^2} \quad (23)$$

At NLO, we estimate the residual uncertainty from missing higher order terms by simultaneously varying μ_r, μ_f over the range:

$$0.5 \times \mu_0 < \mu_r, \mu_f < 2 \times \mu_0. \quad (24)$$

Instructions for using the Effective LRSM at NLO within the MG5_aMC@NLO framework are provided in App. A. For total inclusive cross sections reported in Sec. IV A and IV B, no phase

space cuts are applied. To study the properties of N jets and t jets, we consider the processes

$$p p \rightarrow W_R^{\pm(*)} \rightarrow Ne^{\pm}, tb, \text{ and } qq', \quad \text{for } q \in \{u, d, c, s\}, \quad (25)$$

at NLO in QCD. We include hard QCD radiation off the final-state quarks and a finite W_R width. While we neglect interference with the SM W for simplicity, it is possible to implement it within our framework. To minimize the contamination of far off-shell W_R with virtualities $Q^2 \ll M_{W_R}^2$, we impose a generator-level cut on $X \in \{N, t, q\}$ and require $p_T^X > 750$ GeV. While the cut on light quarks is trivial in MG5_aMC@NLO restrictions on on-shell heavy neutrinos and top quarks require implementing a user-defined cut into the phase space integration routine. This can be done in a straightforward manner; see App. C for instructions.

C. Spin-Correlated Decays of N and t with Improved MadSpin

We decay N and t via MadSpin [56], thus retaining full spin correlation, just before parton showering. However, three body decays like $N \rightarrow \ell^{\pm} W_R^{\mp*} \rightarrow \ell^{\pm} qq'$ are not supported in current releases of MadSpin. Therefore, we have implemented an extension of the code to support such subprocesses. To achieve this, we first use a standard MC technique to generate unweighted decay events with the parent particle being exactly on-shell. Those events are then boosted to match the decaying particle of the production event. Obviously such samples lack spin-correlations between the production event and the decay event. To include spin effects, one can re-weight each decayed event by the following ratio:

$$\frac{|M_{P+D}|^2}{|M_P|^2 |M_D|^2}, \quad (26)$$

where $|M_P|^2$, $|M_D|^2$ and $|M_{P+D}|^2$ are, respectively, the matrix-element squared for the production event, the decay event, and the decayed production event. In order to keep unweighted events after such re-weighting, we follow the MadSpin strategy of keeping the same production event and try associating it with different decay events as long as none of them pass the unweighting criteria. This feature will be include in MG5_aMC@NLO 2.5.3 and is currently available on request. The syntax for enacting such decays is provided in App. B. We note that is also presently possible to perform the three-body heavy N decay with PY8, but at the cost of neglecting spin corrections.

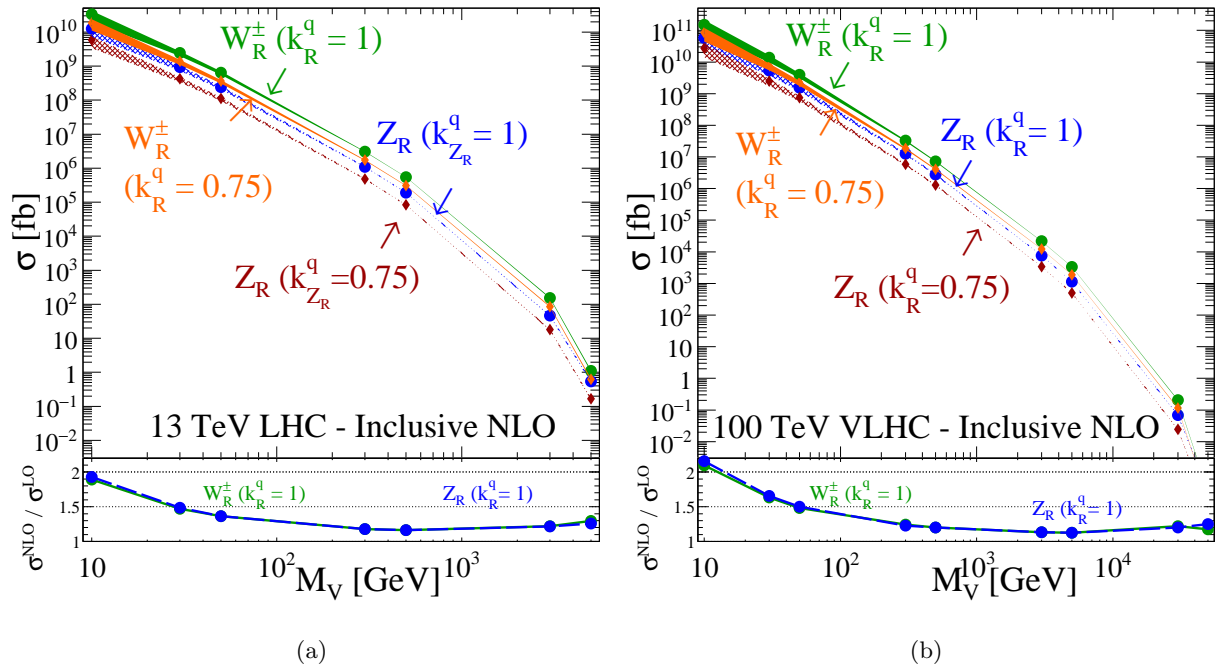


FIG. 3. Total inclusive $pp \rightarrow W_R^\pm$ (solid) and Z_R (hash) NLO production cross section [fb] as a function mass [GeV] at (a) $\sqrt{s} = 13$ and (b) 100 TeV, for different coupling normalizations. Curve widths correspond to residual scale uncertainty. Lower: Ratio of NLO to LO cross sections.

IV. RESULTS

We now report our results for several processes in pp and ep collisions: In Sec. IV A, we present inclusive $pp \rightarrow W_R, Z_R$ production rates at NLO for the LHC and VLHC. In Sec. IV B are the LO rates for inclusive N production in different LHeC configurations. And in Sec. IV C, we present kinematic properties of neutrino jets and top jets originating from W_R decays at the LHC.

A. Inclusive W_R, Z_R Production in Hadron-Hadron Collisions

In Fig. 3, we show the total inclusive $pp \rightarrow W_R^\pm$ (solid) and Z_R (hash) NLO production cross section as a function mass at (a) $\sqrt{s} = 13$ and (b) 100 TeV, for coupling normalizations $\kappa_R^q = 0.75, 1.0$. The curves' widths corresponds to residual scale uncertainty. As the same scale is probed, the uncertainties for the two κ_R^q are identical. In the lower panel are the NLO K -factors,

$$K^{\text{NLO}} \equiv \frac{\sigma^{\text{NLO}}}{\sigma^{\text{LO}}}. \quad (27)$$

We apply our calculations to masses as low as $M_{V_R} = 10$ GeV. While excluded for $\kappa_R^{q,\ell} = 1$, as

$\sigma(pp \rightarrow V_R + X)$ [fb]						
$\sqrt{s} = 13$ TeV						
M_{V_R} [TeV]	$\sigma^{\text{LO}}(W_R)$ [fb]	$\sigma^{\text{NLO}}(W_R)$ [fb]	K^{NLO}	$\sigma^{\text{LO}}(Z_R)$ [fb]	$\sigma^{\text{NLO}}(Z_R)$ [fb]	K^{NLO}
1	3.60×10^4	$4.16^{+1.9\%}_{-1.7\%} \times 10^4$	1.16	1.19×10^4	$1.37^{+2.0\%}_{-1.8\%} \times 10^4$	1.15
3	1.26×10^2	$1.53^{+3.1\%}_{-3.8\%} \times 10^2$	1.21	3.80×10^1	$4.60^{+3.1\%}_{-3.7\%} \times 10^1$	1.21
5	8.38×10^{-1}	$1.10^{+5.4\%}_{-6.4\%}$	1.31	4.26×10^{-1}	$5.49^{+4.4\%}_{-5.3\%} \times 10^{-1}$	1.29
$\sqrt{s} = 100$ TeV						
M_{V_R} [TeV]	$\sigma^{\text{LO}}(W_R)$ [fb]	$\sigma^{\text{NLO}}(W_R)$ [fb]	K^{NLO}	$\sigma^{\text{LO}}(Z_R)$ [fb]	$\sigma^{\text{NLO}}(Z_R)$ [fb]	K^{NLO}
1	7.31×10^5	$8.57^{+2.3\%}_{-3.2\%} \times 10^5$	1.17	2.73×10^5	$3.17^{+2.1\%}_{-3.1\%} \times 10^5$	1.16
5	2.97×10^3	$3.35^{+1.1\%}_{-0.9\%} \times 10^3$	1.13	1.02×10^3	$1.15^{+1.1\%}_{-1.0\%} \times 10^3$	1.13
25	8.34×10^{-1}	$1.00^{+2.5\%}_{-3.2\%}$	1.20	2.62×10^{-1}	$3.09^{+2.3\%}_{-2.9\%} \times 10^{-1}$	1.18
33	6.20×10^{-2}	$7.65^{+3.4\%}_{-4.2\%} \times 10^{-2}$	1.23	2.37×10^{-2}	$2.87^{+2.9\%}_{-3.6\%} \times 10^{-2}$	1.21

TABLE III. Total inclusive LO and NLO (with residual scale dependence [%]) $pp \rightarrow W_R^\pm, Z_R$ cross sections [fb] at $\sqrt{s} = 13$ and 100 TeV for representative M_{W_R}, M_{Z_R} .

reported in Sec. II A, this is not necessarily the case for scenarios with $\kappa_R^{q,\ell} \ll 1$. At both colliders, we observe for $M_{V_R} < 30$ GeV that NLO corrections increase the total cross section by more than 50%, and reach $\sim 100\%$ for $M_{V_R} = 10$ GeV. Such immense corrections are attributed to the large gluon PDF at small x , and leads to a similarly large gq luminosity. Corrections at next-to-next-to-leading order (NNLO) [61] show that the perturbative series is convergent. We note for $M_{V_R}/\sqrt{s} > 0.3$ that the NLO scale uncertainty underestimates the size of additional perturbative corrections. The contribution from resummed threshold corrections in that regime greatly exceed the NLO and NNLO uncertainty bands, and have been found to be at least as large as the NLO corrections [7]. Hence, for extreme values M_{V_R} , the NLO K -factors used in LHC searches [22–25] underestimate W_R, Z_R cross sections. Correcting for PDF and scale choice, we confirm that the predictions of our model file agree with known LO [37, 57, 58] and NLO [7, 61, 62] calculations, as well as Z_R production in ee collisions [59]. We summarize our findings in Tb. III.

In principle, associated top production channels at NLO in QCD, e.g.,

$$pp \rightarrow W_R^\pm t, \quad pp \rightarrow Z_R t \bar{t}, \quad (28)$$

are possible with the model file. However, such radiative processes grow logarithmically as $\sigma \sim$

$\sigma(ep \rightarrow N + X)$ [fb]		
(M_{W_R}, m_N) [TeV, GeV]	$\sigma^{\text{LO}}(E_e = 60 \text{ GeV})$ [fb]	$\sigma^{\text{LO}}(E_e = 140 \text{ GeV})$ [fb]
(3,30)	2.90	6.59
(3,300)	1.05	3.66
(5,500)	4.06×10^{-2}	2.67×10^{-1}
(5,1000)	5.73×10^{-5}	2.33×10^{-2}

TABLE IV. Inclusive LO $ep \rightarrow N$ cross sections [fb] for $E_p = 7$ TeV and alternate E_e configurations, electron polarization of $P_e = +80\%$, and representative (M_{W_R}, m_N) .

$\alpha_s^k(M_V) \log^{(2k-1)}(M_{V_R}^2/m_t^2)$. For $M_{W_R}, M_{Z_R} \gg m_t$, these logarithms lead to numerical instabilities and require either a subtraction scheme to remove double counting of phase space configurations [63–66], or kinematics cuts on final-state tops consistent with Collins-Soper-Sterman perturbativity demands [67] as outlined in [68]. Further discussions of such corrections are beyond the scope of this study.

B. Inclusive N Production in Hadron-Electron Collisions

Proposed multi-TeV deeply inelastic scattering (DIS) experiments, such as the LHeC [39] and eRHIC [75], are well-motivated and can greatly improve our knowledge of PDFs at low- and high- x , resummed QCD, and EW couplings. Additionally, due to the cleanliness of the collider environment (in comparison to pp collisions) and the increased c.m.e reach over the LHC, the LHeC offers a complementary opportunity to search for new physics. In particular, the LHeC is capable of probing regions of LRSM parameter space inaccessible to the LHC [69–72].

The LRSM can be tested at the LHeC through searches for heavy N through the process,

$$e^- p \rightarrow N j + X, \quad \text{where } N \rightarrow \ell'^{\pm} q \bar{q}', \quad (29)$$

which is mediated by t -channel W_R exchange and is shown in Fig. 2(b). Initial search strategies [71, 72] have proposed requiring three high- p_T jets in the central region of the detector. Two arise from the decay of N , the third from the associated W_R exchange. We argue that the requirement of a third jet is unnecessary and likely reduces N discovery potential: Eq. (29) involves the exchange of a gauge boson with a mass much larger than the collider, and hence momentum transfer scale, i.e., $M_{W_R}^2 \gg |\hat{t}|$. This implies that the spectator jet has no natural momentum scale, unlike the

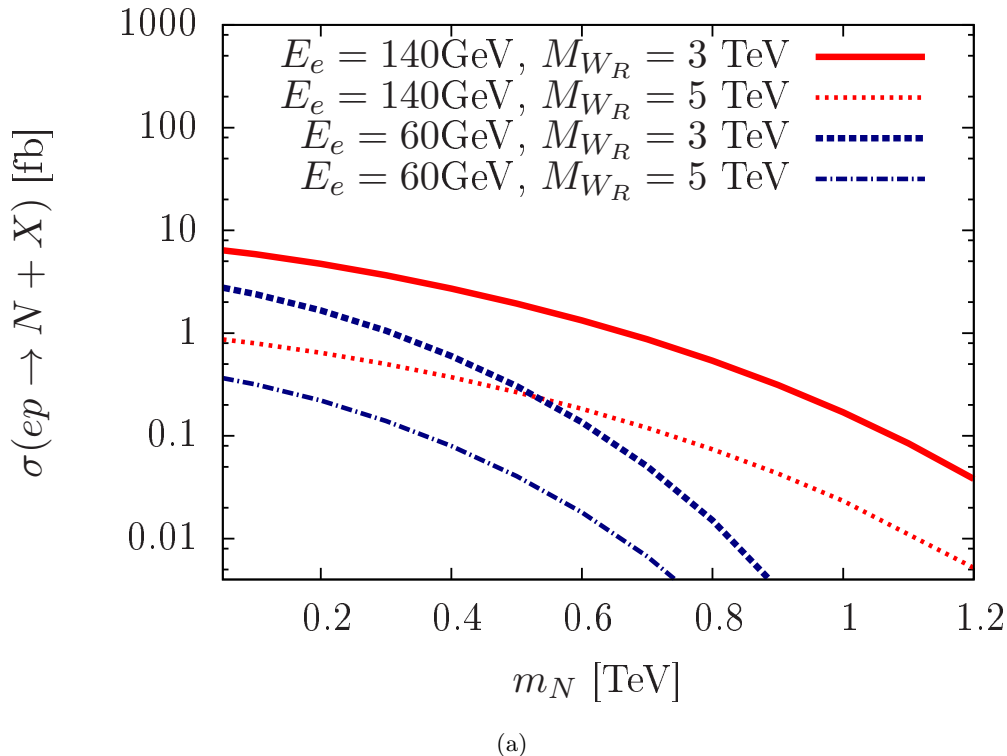


FIG. 4. The LO inclusive $e^-p \rightarrow N + X$ cross section as function of N mass for different LHeC beam configurations.

decay products of N , which scale like m_N . Subsequently, a large (and entirely finite) region of the phase space is populated by forward, low- p_T jets that do not satisfy the selection criteria of [71, 72]. Furthermore, this spectator is not necessary to reconstruct the heavy neutrino momentum. We therefore recommend a more inclusive approach, and propose instead the search

$$e^- p \rightarrow N + X, \quad \text{where } N \rightarrow \ell'^{\pm} q \bar{q}'. \quad (30)$$

As a function of m_N , we show in Fig. 4 the inclusive cross section at LO for Eq. (30) with representative M_{W_R} and proposed beam configurations [39, 72]. For select (M_{W_R}, m_N) , we summarize our findings in Tb. IV. We defer a detailed signal-vs-background investigation to a future study.

Automated NLO in QCD corrections are not yet possible within the MG5_aMC@NLO framework for ep collisions. As this is presently possible for pp and ee beam configurations, the issue is merely technical rather than conceptual. We note though that while total inclusive rates remain essentially unchanged at NLO for DIS processes, this is not true differentially as studies of vector boson fusion beyond LO+PS have shown [68, 73, 74]. We advocate for such a computational abilities in order to accurately assess the physics potential of future high energy DIS.

C. Kinematics of Neutrino and Top Jets at NLO+PS in LHC Collisions

Heavy neutrinos and top quarks originating from W_R (or Z_R) decays carry characteristic transverse momenta that scale as $p_T \sim M_{W_R}/2$. For $M_{W_R} \gg m_{N,t}$, such neutrinos and tops are highly Lorentz boosted. Subsequently, their decays to leptons and/or quarks, as shown in Fig. 5, are highly collimated, and lead to the formation of heavy neutrino jets [6, 7] and top quark jets [26–28].

In this section we compare kinematics of neutrino, top, and light quark jets from high-mass M_{W_R} decays at NLO+PS accuracy. We describe our computational setup in Sec. III. The $N \rightarrow \ell^\pm q\bar{q}'$ branching fraction is 100%; for t , we allow both hadronic and leptonic decays of the SM W .

Events topologies are studied by first identifying charged lepton candidates, then clustering all residual objects, including potentially misidentified leptons, into jets. Stable charged leptons $\ell \in \{e, \mu\}$ are considered hadronically isolated if the scalar sum of transverse energy (E_T) over all neighboring hadrons X within a distance of $\Delta R_{\ell X} < 0.3$ is less than 10% of the lepton's E_T , i.e.,

$$\sum_{X \in \{\text{hadrons}\}} E_T^X / E_T^\ell < 0.1 \quad \text{for} \quad \Delta R_{\ell X} < 0.3. \quad (31)$$

At the 13 TeV LHC, charged lepton candidates are then defined as hadronically isolated leptons that meet the following kinematic, fiducial, and lepton isolation requirements [76]:

$$p_T^\ell > 35 \text{ GeV}, \quad |\eta^\ell| < 2.4, \quad \Delta R_{\ell\ell'} > 0.3. \quad (32)$$

We cluster all remaining constituents into jets according to the Cambridge/Aachen (C/A) algorithm [77, 78] with a separation scale of $R = 1.0$. We ignore clustered jets with $p_T < 20$ GeV [79]. Charged leptons and jets are ordered according to their p_T (hardness), with $p_T^{j_i} > p_T^{j_{(i+1)}}$. To select for top quarks and heavy neutrinos, we apply the following mass cut on the hardest jet, j_1 :

$$|m_{j_1} - m_t| < 25 \text{ GeV}. \quad (33)$$

The NLO+PS accurate cross section before and after the jet mass cut are:

$$\sigma^{\text{NLOPS}} : \quad 14.0 \text{ (36.7) [76.3] fb} \quad \text{for the } N \text{ (} t \text{) [} q \text{] channel,} \quad (34)$$

$$\sigma^{\text{NLOPS}+m_j \text{ Cut}} : \quad 8.39 \text{ (9.69) [9.16] fb} \quad \text{for the } N \text{ (} t \text{) [} q \text{] channel} \quad (35)$$

We see that the m_j (accidentally) brings the individual rates to a very comparable level, avoid the need for any additional type of normalization. Without the cut, the quark channels are much larger due to branching fractions that are $3 - 6\times$ larger. To reconstruct W_R kinematics, we drop the jet mass cut and sum the momenta of the two hardest jets in the quark channels, or hardest jet and lepton in the neutrino channel.

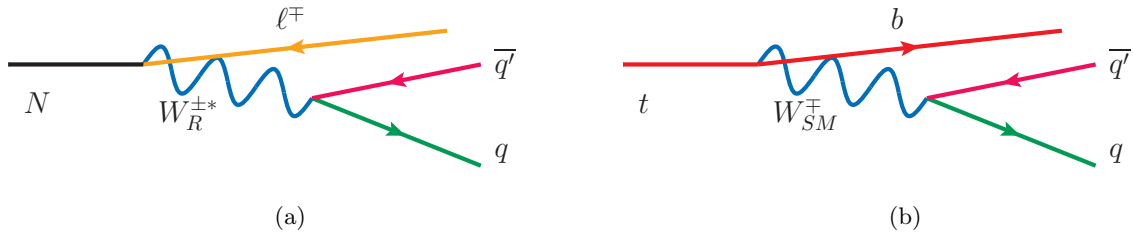


FIG. 5. Leading decay modes for (a) N and (b) t in the LRSM.

In Fig. 6 we plot at NLO+PS accuracy, the differential distributions of various observables related to j_1 in W_R production and decay to heavy neutrino (solid), top quark (dash), and light quark (dot) jets, at the $\sqrt{s} = 13$ TeV LHC. For observable \mathcal{O} , the lower panel shows the differential NLO+PS K -factor, defined as the ratio

$$K_{\mathcal{O}}^{\text{NLO+PS}} \equiv \frac{d\sigma^{\text{NLO+PS}}/d\mathcal{O}}{d\sigma^{\text{LO+PS}}/d\mathcal{O}}. \quad (36)$$

In Fig. 6(a), we show the p_T distribution of j_1 . The Jacobian peak at $p_T \sim M_{W_R}/2 \sim 1.5$ TeV is clearly visible, but is noticeably broader for t and q jets than N jets. With respect to LO+PS, quark jets possess a varying differential K -Factor that falls below 1 for $p_T \lesssim 1$ TeV, and grows to $K_{p_T}^{\text{NLO+PS}} \sim 1.2$ for larger p_T . For neutrino jets, $K_{p_T}^{\text{NLO+PS}} \approx 1.2$ and is approximately constant across all p_T . Numerically, $K_{p_T}^{\text{NLO+PS}} \approx 1.2$ is very close to the total inclusive NLO K -factor for W_R production, which is driven by virtual and soft corrections. We attribute the differences in broadening and $K_{p_T}^{\text{NLO+PS}}$ simply to the fact that quarks carry net color charge, unlike neutrinos: Quark jets are susceptible to hard, wide-angle FSR that carry away momentum and causes broadening in the p_T spectrum. In DY-type processes, this is more accurately modeled by matrix element corrections that first appear at NLO in QCD than by parton showers.

In Fig. 6(b) is the rapidity (y) distribution of j_1 . Compared to quark jets, heavy neutrino jets possesses a broader, flatter distribution. With respect to LO+PS, again, $K_{p_T}^{\text{NLO+PS}} \approx 1.2$ and is approximately constant for neutrino jets. For quarks jets, we observe a depletion of events with larger rapidities, and is consistent with the p_T spectrum at NLO+PS.

We show in Fig. 6(c) the jet mass distribution centered about m_t . For heavy neutrino and top jets, the resonant peak around m_t is unambiguous. As the light quark jet contribution is a continuum at this mass scale, it is featureless. Most striking is the upward shift in the top jet mass compared to the neutrino jet mass. The shift is caused, in part, by the production of an off-shell top that then emits a (semi-)collinear radiation and is brought on-shell. The collinear nature of

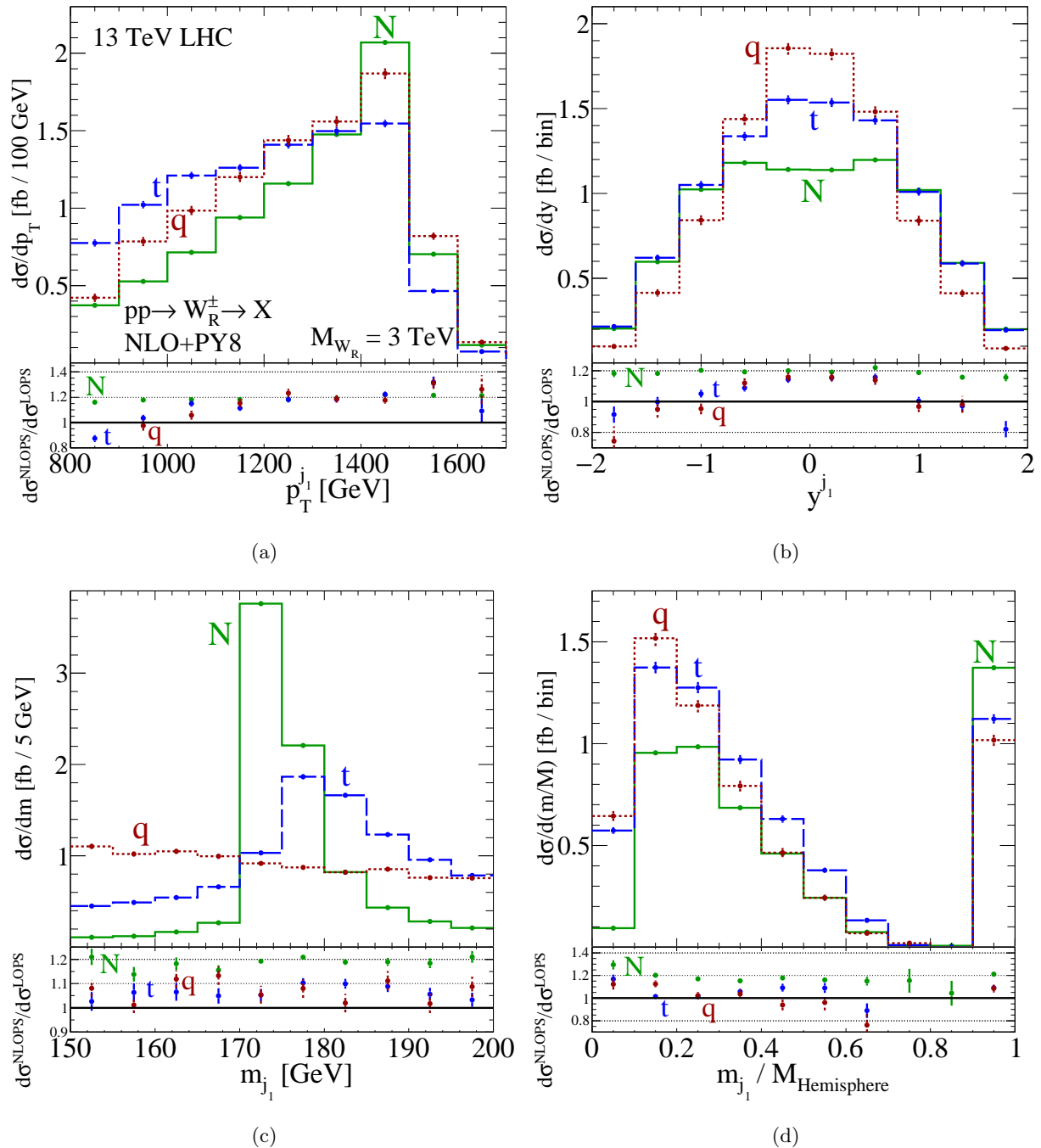


FIG. 6. Differential distributions with respect to (a) $p_T^{j_1}$, (b) y^{j_1} , (c) m_{j_1} , and the (d) $m_{j_1}/M_{\text{Hemisphere}}$ ratio, at NLO+PS, of W_R production and decay to heavy neutrino (solid), top quark (dash), and light quark (dot) jets, at the $\sqrt{s} = 13$ TeV LHC. m_{j_1} cut applied. Lower: NLO+PS-to-LO+PS ratio.

the emission means it is captured by the sequential jet algorithm and is well-modeled by parton showers. As $M_{W_R} \gg m_t$, such a configuration is not phase space suppressed. Non-perturbative and large finite width effects are also important[80, 81]. For more details, see, e.g., [80, 81] and

references therein. However, as neutrinos are not subject to such effects, N jets retains their narrow, resonant structure, even after showering and hadronization. This suggests that searches for neutrino jets, as proposed by [6, 7], may be able to impose much more aggressive invariant mass cuts than the 15 GeV presently used in LHC top quark mass studies [82].

In Fig. 6(d) we plot the ratio of $m_{j_1}/M_{\text{Hemisphere}}$, where $M_{\text{Hemisphere}}$ is the hemisphere mass associated with j_1 . We define the hemisphere mass of the leading jet simply as the invariant mass of all jet momenta p_k in the same hemisphere as j_1 , i.e.,

$$M_{\text{Hemisphere}} = \sqrt{p_{\text{Hemisphere}}^2}, \quad \text{where } p_{\text{Hemisphere}} = \sum_{k \in \{\text{jets}\}} p_k \quad \text{and} \quad \hat{p}_k \cdot \hat{p}_{j_1} > 1. \quad (37)$$

Due to the large W_R mass we consider, it is largely at rest in $\sqrt{s} = 13$ TeV collisions. This is supported by Fig. 7(a). Subsequently, while not rigorously infrared-collinear safe, the axis defined by the direction of hardest jet is the thrust axis to a good approximation, justifying the use of Eq. (37). The utility of this ratio is its sensitivity to radiation associated with a parton but missed by a jet algorithm because the emission angle is too wide, e.g., high- p_T , wide angle FSR off a top quark that falls outside the top jet’s radius. Due to the presence of non-global logarithms and jet substructure, as well as parton shower dependence, a complete and systematic study of hemisphere variables is outside the narrow scope of this report. For further details, see [83–86] and references therein. In the context of the C/A algorithm, the ratio can be interpreted as the mass ratio of a jet with $R = 1$ to that of a “larger” jet with $R \approx \pi/2$. In all three channels, we find a sizable fraction of events are concentrated at $0.9 < m_{j_1}/M_{\text{Hemisphere}} < 1$, indicating that single the hardest jet from high-mass W_R decays contains most all the radiation one one side of the detector. As expected, fewer quark jet events satisfy this property. The accumulation at smaller ratios is due to the large contamination from ISR, which is supported by the flat N jet differential K -factor.

In Fig. 7 we show the kinematics of the reconstructed W_R system built from the $(j_1 j_2)$ and $(\ell^\pm j)$ systems for the quark and neutrino channels, respectively. No jet mass cuts are applied. In (a), (b), (c), and (d), we show respectively, $p_T^{W_R^{\text{Reco.}}}$, $y^{W_R^{\text{Reco.}}}$, $M_{W_R^{\text{Reco.}}}$, and the polar distribution of j_1 in the $W_R^{\text{Reco.}}$ ’s rest frame. Due to bin resolution, the Sudakov shoulder in the p_T spectrum is not shown. In the invariant mass distribution, we find sizable broadening in the quark channels of the W_R mass peak due to hard, wide-angle FSR; this is largely absent for neutrinos.

Categorically, we observe that neutrino jets possess largely constant differential K -factors. This is qualitatively different from quark jets, which feature more dynamical $K_{\mathcal{O}}$. The result follows from the color-singlet nature of the $pp \rightarrow W_R^\pm \rightarrow Ne^\pm$ process and large mass (in comparison to the total beam c.m. energy) of the intermediate W_R : Since N and e are color neutral, they do not

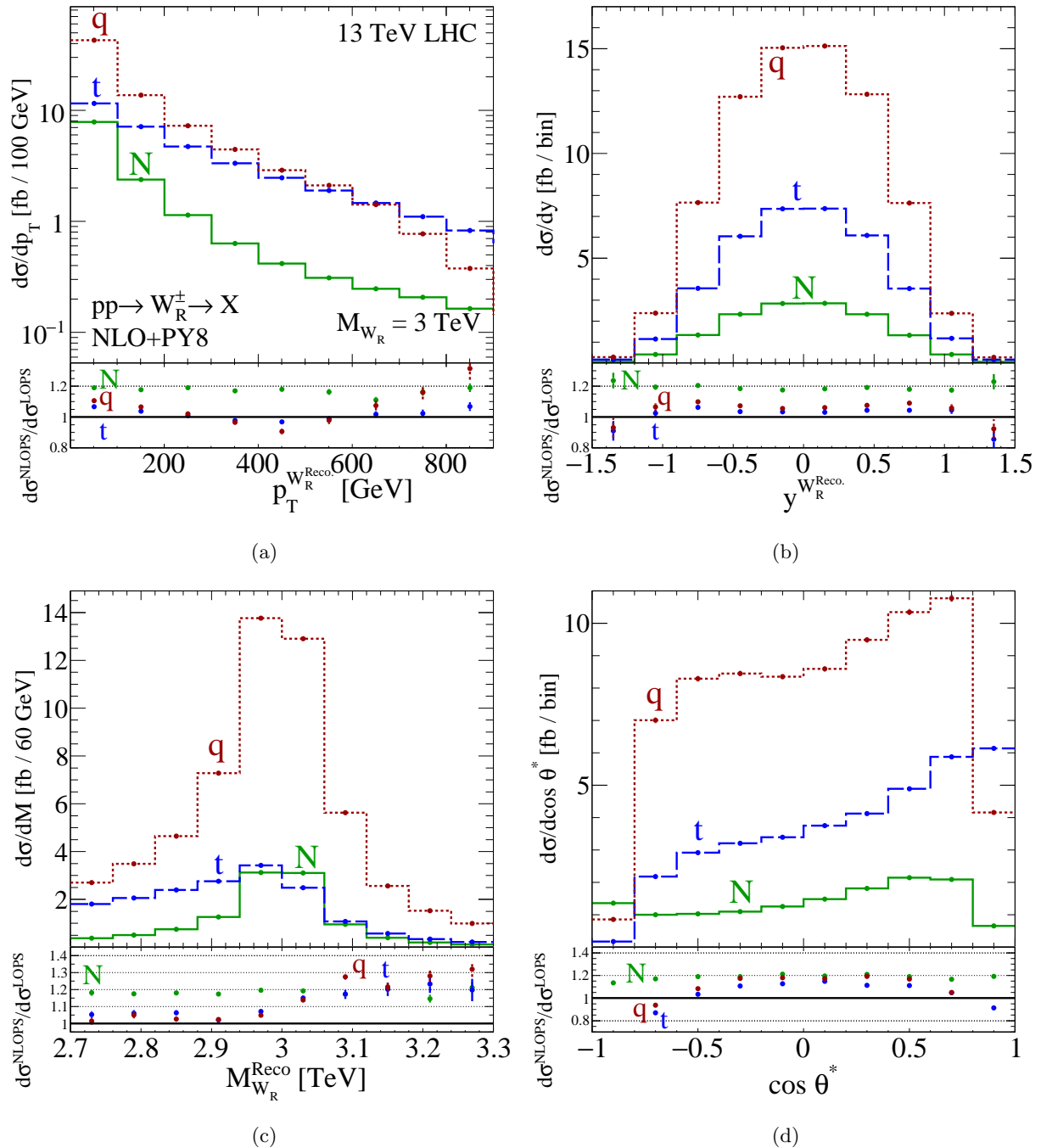


FIG. 7. Kinematic distributions of the reconstructed W_R system with respect to (a) $p_T^{W_R^{\text{Reco.}}}$, (b) $y^{W_R^{\text{Reco.}}}$, (c) $M_{W_R^{\text{Reco.}}}$, and (d) the polar distribution of j_1 in the $W_R^{\text{Reco.}}$'s rest frame for the same configuration as Fig. 6. No m_{j_1} cut applied. Lower: NLO+PS-to-LO+PS ratio.

undergo QCD FSR, implying that all QCD corrections are confined to the $q\bar{q}' \rightarrow W_R^*$ subprocess. However, due to the large M_{W_R} considered, high- p_T ISR is phase space-suppressed, leaving only hard-collinear (HC) and soft ISR. HC radiation is encapsulated in the definitions of PDFs and

parton showers, and therefore is the same at LO and NLO. For high-mass DY processes, in both the SM and generic BSM scenarios, virtual corrections and soft radiation amplitudes factorize into the Born amplitude and universal form factors that combine (due to the KLN theorem) into a finite QCD scaling factor. Subsequently, total and differential NLO in QCD K -factors for high-mass DY systems are constant, up to running of $\alpha_s(\mu)$.

V. SUMMARY AND CONCLUSION

The LRSM is a predictive and economic extension of the SM that explains several observations not accommodated by the SM. It postulates the existence of the W_R, Z_R , gauge bosons and Majorana neutrinos N , that may be discovered/studied at the LHC or near-future collider experiment.

We report the construction of a new MC model file capable of simulating fully differential benchmark W_R, Z_R , and N production and decay processes at an accuracy up to NLO+PS using the FR+MG5_aMC@NLO+PY8 framework. Such corrections are necessary to realistically model QCD radiation at hadron super colliders. Remarkably fewer input parameters are required in comparison to LO LRSM implementations. Publicly available UFO files [34] are compatible with similar general-purpose event generators, e.g., HERWIG and SHERPA.

Our NLO in QCD corrections and residual scale uncertainty for inclusive $pp \rightarrow W_R, Z_R$ production at the 13 TeV LHC and 100 TeV VLHC are in agreement with other findings. This is similarly the case for inclusive $e^-p \rightarrow N + X$ production at a future LHeC experiment.

As a case study, we have investigated at NLO+PS accuracy, the kinematics of heavy neutrino jets and top jets originating from the decay of high-mass W_R decays at the 13 TeV LHC. With respect to LO+PS, we find appreciable changes to top jet kinematics that we attribute hard, wide-angle FSR not captured by parton showers. Conversely, due to the absence of such FSR, we find neutrino jets kinematics are resilient against the effects of parton showers and hadronization. This suggests that in searches for neutrino jets, aggressive selection cuts that would otherwise be inappropriate for top jets can be imposed with minimal signal loss.

ACKNOWLEDGMENTS

Johannes Bellm, Mrinal Dasgupta, Simon Platzer, Darren Scott, and Michael Spannowsky are thanked for discussions. Catherine Theriault and Aaron Vincent are thanked for their maple syrup. This work was supported by UK Science and Technology Facilities Council (STFC), the Belgian Pole d'attraction Inter-Universitaire (PAI P7/37), and the European Union's Horizon 2020 research and innovation programme under the Marie Skłodowska-Curie grant agreements Nos. 690575, 674896, 690575 (InvisiblesPlus RISE), and 674896 (Elusives ITN). OM would like to thank the CERN TH division for its hospitality. RR would like to thank the IHEP Theory group for its hospitality and support.

Appendix A: EffLRSM@NLO Signal Simulation with MG5_aMC@NLO

In this section, we provide brief instructions for simulating particle production in the Effective LRSM using the MG5_aMC@NLO+PY8 framework for FO and PS predictions.

The inclusive $pp \rightarrow W_R$ cross section at NLO can be calculated for $M_{W_R} \in [1 \text{ TeV}, 6 \text{ TeV}]$ in 1 TeV increments with the scale choice of Eq. (23) via the MG5_aMC@NLO commands:

```
> import model EffLRSM_NLO
> define p = u c d s b u~ c~ d~ s~ b~ g
> define j = p
> define wr = wr+ wr-
> generate p p > wr [QCD]
> output PP_WR_NLO; launch
> order=NLO
> fixed_order=ON
> set MWR scan:range(1000,6001,1000)
> set dynamical_scale_choice 3
```

In the same environment, the LO cross section at, say, 100 TeV can be computed with the following:

```
> launch PP_WR_NLO
```

```
> order=L0
> set LHC 100
```

Inclusive $pp \rightarrow Z_R$ production rates are obtained by making the obvious $wr \rightarrow zr$ substitution.

To simulate $pp \rightarrow W_R \rightarrow Ne^\pm$ at NLO+PS with finite W_R width effects, the commands are:

```
> generate p p > wr+ > n1 e+ [QCD]
> add process p p > wr- > n1 e- [QCD]
> output PP_WR_Ne_NLO; launch
```

Other leptons, e.g., N_2 or τ^\pm , can appear in the final state but may require regeneration of the LRSM UFO; default lepton mixing is set according to Eq. (7). For $W_R^* \rightarrow tb$, the commands are:

```
> generate p p > wr+ > t b~ [QCD]
> add process p p > wr- > t~ b [QCD]
> output PP_WR_tb_NLO; launch
```

Simulating inclusive $e^-p \rightarrow N+X$ production at LO for $M_{W_R} = 3$ TeV and $m_N \in [100 \text{ GeV}, 1 \text{ TeV}]$ in 100 GeV increments can be done using the following:

```
> generate generate e- p > n1 j
> output PP_ep_NX_LO; launch
> set lpp1 0
> set ebeam1 140
> set ebeam2 7000
> set polbeam1 80
> set MWR 3000
> set mn1 scan:range(100,1001,100)
```

The third line turns off the PDF for the electron beam, whereas the fourth and fifth line sets the individual beam energies. The line after sets the electron beam polarization to $P_e = +80\%$.

Appendix B: Three-Body Decays of N and t in MadSpin

As shown in Fig. 5, decays of the lightest heavy neutrino in the LRSM are dominated by the process $N \rightarrow \ell^\pm W_R^{\mp*} \rightarrow \ell^\pm q\bar{q}$. Here W_R is far off-shell. To model such processes using MadSpin within the MG5_aMC@NLO framework requires adding to `Cards/madspin_card.dat` the following:

```

set spinmode onshell
define q = u c d s u~ c~ d~ s~
define ee = e+ e-
decay n1 > ee q q
launch

```

For top quarks decaying to hadronic and leptonic final states, we use the following MadSpin syntax:

```

decay t > w+ b, w+ > all all
decay t~ > w- b~, w- > all all
launch

```

In both cases, we retain full spin correlation with the hard process matrix elements.

Appendix C: User Defined Generator-Level Cuts in MG5_aMC@NLO

Imposing phase space cuts on final-state top quarks and heavy neutrinos in MG5_aMC@NLO requires modifying the file `SubProcesses/cuts.f` in the local process directory, i.e., the directory `PP_WR_Ne_NLO` or `PP_WR_tb_NLO` if following App. A. To apply our generator-level cut of $p_T > 750$ GeV with NLO in QCD accuracy, we insert after Line 377 of `cuts.f` the following:

```

do i=1,nexternal          ! loop over all external particles
  if (istatus(i).eq.1 .and. ! check if final-state particle and
& (abs(ipdg(i)).eq.6 .or.   ! PID == top quark or
& abs(ipdg(i)).eq.9900012) ! PID == heavy neutrino
& ) then
C Reject event if pT < 750 GeV
  if ( p(1,i)**2+p(2,i)**2 .lt. (750.0d0)**2 ) then
    passcuts_user=.false.
    return
  endif
endif
enddo

```

-
- [1] J. C. Pati and A. Salam, “Lepton Number as the Fourth Color” Phys. Rev. D **10**, 275 (1974) Erratum: [Phys. Rev. D **11**, 703 (1975)]. doi:10.1103/PhysRevD.10.275, 10.1103/PhysRevD.11.703.2
- [2] R. N. Mohapatra and J. C. Pati, “A Natural Left-Right Symmetry” Phys. Rev. D **11**, 2558 (1975). doi:10.1103/PhysRevD.11.2558
- [3] G. Senjanovic and R. N. Mohapatra, “Exact Left-Right Symmetry and Spontaneous Violation of Parity” Phys. Rev. D **12**, 1502 (1975). doi:10.1103/PhysRevD.12.1502
- [4] D. Binosi and L. Theussl, “JaxoDraw: A Graphical user interface for drawing Feynman diagrams,” Comput. Phys. Commun. **161**, 76 (2004) [hep-ph/0309015].
- [5] W. Y. Keung and G. Senjanovic, “Majorana Neutrinos and the Production of the Right-handed Charged Gauge Boson,” Phys. Rev. Lett. **50**, 1427 (1983). doi:10.1103/PhysRevLett.50.1427
- [6] A. Ferrari, J. Collot, M. L. Andrieux, B. Belhorma, P. de Saintignon, J. Y. Hostachy, P. Martin and M. Wielers, “Sensitivity study for new gauge bosons and right-handed Majorana neutrinos in pp collisions at $s = 14$ -TeV,” Phys. Rev. D **62**, 013001 (2000). doi:10.1103/PhysRevD.62.013001
- [7] M. Mitra, R. Ruiz, D. J. Scott and M. Spannowsky, “Neutrino Jets from High-Mass W_R Gauge Bosons in TeV-Scale Left-Right Symmetric Models,” arXiv:1607.03504 [hep-ph].
- [8] E. H. Simmons, “New gauge interactions and single top quark production,” Phys. Rev. D **55**, 5494 (1997) doi:10.1103/PhysRevD.55.5494 [hep-ph/9612402].
- [9] M. Frank, A. Hayreter and I. Turan, “Production and Decays of W_R bosons at the LHC” Phys. Rev. D **83**, 035001 (2011) doi:10.1103/PhysRevD.83.035001 [arXiv:1010.5809 [hep-ph]].
- [10] V. Tello, M. Nemevsek, F. Nesti, G. Senjanovic and F. Vissani, “Left-Right Symmetry: from LHC to Neutrinoless Double Beta Decay,” Phys. Rev. Lett. **106**, 151801 (2011) [arXiv:1011.3522 [hep-ph]].
- [11] S. P. Das, F. F. Deppisch, O. Kittel and J. W. F. Valle, “Heavy Neutrinos and Lepton Flavour Violation in Left-Right Symmetric Models at the LHC” Phys. Rev. D **86**, 055006 (2012) doi:10.1103/PhysRevD.86.055006 [arXiv:1206.0256 [hep-ph]].
- [12] T. Han, I. Lewis, R. Ruiz and Z. g. Si, “Lepton Number Violation and W' Chiral Couplings at the LHC” Phys. Rev. D **87**, no. 3, 035011 (2013) doi:10.1103/PhysRevD.87.035011, [arXiv:1211.6447 [hep-ph]].
- [13] C. Y. Chen, P. S. B. Dev and R. N. Mohapatra, “Probing Heavy-Light Neutrino Mixing in Left-Right Seesaw Models at the LHC,” Phys. Rev. D **88**, 033014 (2013) doi:10.1103/PhysRevD.88.033014 [arXiv:1306.2342 [hep-ph]].
- [14] J. C. Vasquez, JHEP **1605**, 176 (2016) doi:10.1007/JHEP05(2016)176 [arXiv:1411.5824 [hep-ph]].
- [15] A. Maiezza, M. Nemevsek and F. Nesti, “Lepton Number Violation in Higgs Decay at LHC” Phys. Rev. Lett. **115**, 081802 (2015) doi:10.1103/PhysRevLett.115.081802 [arXiv:1503.06834 [hep-ph]].
- [16] J. Gluza and T. Jeliński, “Heavy neutrinos and the $p\bar{p}l\bar{l}j$ CMS data” Phys. Lett. B **748**, 125 (2015) doi:10.1016/j.physletb.2015.06.077 [arXiv:1504.05568 [hep-ph]].

- [17] J. N. Ng, A. de la Puente and B. W. P. Pan, “Search for Heavy Right-Handed Neutrinos at the LHC and Beyond in the Same-Sign Same-Flavor Leptons Final State,” *JHEP* **1512**, 172 (2015) doi:10.1007/JHEP12(2015)172 [arXiv:1505.01934 [hep-ph]].
- [18] P. S. B. Dev, D. Kim and R. N. Mohapatra, “Disambiguating Seesaw Models using Invariant Mass Variables at Hadron Colliders,” *JHEP* **1601**, 118 (2016) doi:10.1007/JHEP01(2016)118 [arXiv:1510.04328 [hep-ph]].
- [19] Z. Kang, P. Ko and J. Li, “New Avenues to Heavy Right-handed Neutrinos with Pair Production at Hadronic Colliders,” *Phys. Rev. D* **93**, no. 7, 075037 (2016) doi:10.1103/PhysRevD.93.075037 [arXiv:1512.08373 [hep-ph]].
- [20] J. Chakraborty, J. Gluza, T. Jeliński and T. Srivastava, “Theoretical constraints on masses of heavy particles in Left-Right Symmetric Models” *Phys. Lett. B* **759**, 361 (2016) doi:10.1016/j.physletb.2016.05.092 [arXiv:1604.06987 [hep-ph]].
- [21] P. Fileviez Perez, C. Murgui and S. Ohmer, “Simple Left-Right Theory: Lepton Number Violation at the LHC,” *Phys. Rev. D* **94**, no. 5, 051701 (2016) doi:10.1103/PhysRevD.94.051701 [arXiv:1607.00246 [hep-ph]].
- [22] G. Aad *et al.* [ATLAS Collaboration], “Search for new phenomena in dijet mass and angular distributions from pp collisions at $\sqrt{s} = 13$ TeV with the ATLAS detector” *Phys. Lett. B* **754**, 302 (2016) doi:10.1016/j.physletb.2016.01.032 [arXiv:1512.01530 [hep-ex]].
- [23] V. Khachatryan *et al.* [CMS Collaboration], “Search for narrow resonances decaying to dijets in proton-proton collisions at $\sqrt{s} = 13$ TeV” *Phys. Rev. Lett.* **116**, no. 7, 071801 (2016) doi:10.1103/PhysRevLett.116.071801 [arXiv:1512.01224 [hep-ex]].
- [24] G. Aad *et al.* [ATLAS Collaboration], “Search for heavy Majorana neutrinos with the ATLAS detector in pp collisions at $\sqrt{s} = 8$ TeV” *JHEP* **1507**, 162 (2015) doi:10.1007/JHEP07(2015)162 [arXiv:1506.06020 [hep-ex]].
- [25] V. Khachatryan *et al.* [CMS Collaboration], “Search for heavy neutrinos and W bosons with right-handed couplings in proton-proton collisions at $\sqrt{s} = 8$ TeV” *Eur. Phys. J. C* **74**, no. 11, 3149 (2014) doi:10.1140/epjc/s10052-014-3149-z [arXiv:1407.3683 [hep-ex]].
- [26] U. Baur and L. H. Orr, *Phys. Rev. D* **76**, 094012 (2007) doi:10.1103/PhysRevD.76.094012 [arXiv:0707.2066 [hep-ph]].
- [27] J. Thaler and L. T. Wang, “Strategies to Identify Boosted Tops,” *JHEP* **0807**, 092 (2008) doi:10.1088/1126-6708/2008/07/092 [arXiv:0806.0023 [hep-ph]].
- [28] D. E. Kaplan, K. Rehermann, M. D. Schwartz and B. Tweedie, “Top Tagging: A Method for Identifying Boosted Hadronically Decaying Top Quarks,” *Phys. Rev. Lett.* **101**, 142001 (2008) doi:10.1103/PhysRevLett.101.142001 [arXiv:0806.0848 [hep-ph]].
- [29] A. Alloul, N. D. Christensen, C. Degrande, C. Duhr and B. Fuks, “FeynRules 2.0 - A complete toolbox for tree-level phenomenology,” *Comput. Phys. Commun.* **185**, 2250 (2014) [arXiv:1310.1921 [hep-ph]].

- [30] N. D. Christensen and C. Duhr, “FeynRules - Feynman rules made easy,” *Comput. Phys. Commun.* **180**, 1614 (2009) [arXiv:0806.4194 [hep-ph]].
- [31] C. Degrande, “Automatic evaluation of UV and R2 terms for beyond the Standard Model Lagrangians: a proof-of-principle,” *Comput. Phys. Commun.* **197**, 239 (2015) doi:10.1016/j.cpc.2015.08.015 [arXiv:1406.3030 [hep-ph]].
- [32] J. Alwall *et al.*, “The automated computation of tree-level and next-to-leading order differential cross sections, and their matching to parton shower simulations,” *JHEP* **1407**, 079 (2014) doi:10.1007/JHEP07(2014)079 [arXiv:1405.0301 [hep-ph]].
- [33] C. Degrande, C. Duhr, B. Fuks, D. Grellscheid, O. Mattelaer and T. Reiter, “UFO - The Universal FeynRules Output,” *Comput. Phys. Commun.* **183**, 1201 (2012) doi:10.1016/j.cpc.2012.01.022 [arXiv:1108.2040 [hep-ph]].
- [34] R. Ruiz, “Effective LRSM@NLO” ,<http://feynrules.irmp.ucl.ac.be/wiki/EffLRSM>
- [35] T. Sjostrand, S. Mrenna and P. Z. Skands, “PYTHIA 6.4 Physics and Manual,” *JHEP* **0605**, 026 (2006) doi:10.1088/1126-6708/2006/05/026 [hep-ph/0603175].
- [36] M. Ashry and S. Khalil, “Phenomenological aspects of a TeV-scale alternative left-right model,” *Phys. Rev. D* **91**, no. 1, 015009 (2015) doi:10.1103/PhysRevD.91.015009 [arXiv:1310.3315 [hep-ph]].
- [37] A. Roitgrund, G. Eilam and S. Bar-Shalom, “Implementation of the left-right symmetric model in FeynRules/CalcHep,” arXiv:1401.3345 [hep-ph].
- [38] N. Arkani-Hamed, T. Han, M. Mangano and L. T. Wang, “Physics Opportunities of a 100 TeV Proton-Proton Collider,” arXiv:1511.06495 [hep-ph].
- [39] J. L. Abelleira Fernandez *et al.* [LHeC Study Group Collaboration], “A Large Hadron Electron Collider at CERN: Report on the Physics and Design Concepts for Machine and Detector,” *J. Phys. G* **39**, 075001 (2012) doi:10.1088/0954-3899/39/7/075001 [arXiv:1206.2913 [physics.acc-ph]].
- [40] A. Atre, T. Han, S. Pascoli and B. Zhang, “The Search for Heavy Majorana Neutrinos” *JHEP* **0905**, 030 (2009) doi:10.1088/1126-6708/2009/05/030 [arXiv:0901.3589 [hep-ph]].
- [41] J. Barry and W. Rodejohann, *Lepton number and flavour violation in TeV-scale left-right symmetric theories with large left-right mixing*, *JHEP* **1309**, 153 (2013) doi:10.1007/JHEP09(2013)153 [arXiv:1303.6324 [hep-ph]].
- [42] A. Maiezza and M. Nemevsek, *Strong P invariance, neutron electric dipole moment, and minimal left-right parity at LHC*, *Phys. Rev. D* **90**, no. 9, 095002 (2014) doi:10.1103/PhysRevD.90.095002 [arXiv:1407.3678 [hep-ph]].
- [43] S. Bertolini, A. Maiezza and F. Nesti, *Present and Future K and B Meson Mixing Constraints on TeV Scale Left-Right Symmetry*, *Phys. Rev. D* **89**, no. 9, 095028 (2014) doi:10.1103/PhysRevD.89.095028 [arXiv:1403.7112 [hep-ph]].
- [44] A. Maiezza, M. Nemevek and F. Nesti, arXiv:1603.00360 [hep-ph].
- [45] T. Hahn, “Generating Feynman diagrams and amplitudes with FeynArts 3,” *Comput. Phys. Commun.* **140**, 418 (2001) doi:10.1016/S0010-4655(01)00290-9 [hep-ph/0012260].

- [46] J. Bellm *et al.*, “Herwig 7.0/Herwig++ 3.0 release note,” *Eur. Phys. J. C* **76**, no. 4, 196 (2016) doi:10.1140/epjc/s10052-016-4018-8 [arXiv:1512.01178 [hep-ph]].
- [47] T. Gleisberg, S. Hoeche, F. Krauss, M. Schonherr, S. Schumann, F. Siegert and J. Winter, “Event generation with SHERPA 1.1,” *JHEP* **0902**, 007 (2009) doi:10.1088/1126-6708/2009/02/007 [arXiv:0811.4622 [hep-ph]].
- [48] T. Sjostrand *et al.*, “An Introduction to PYTHIA 8.2,” *Comput. Phys. Commun.* **191**, 159 (2015) doi:10.1016/j.cpc.2015.01.024 [arXiv:1410.3012 [hep-ph]].
- [49] E. Conte, B. Fuks and G. Serret, “MadAnalysis 5, A User-Friendly Framework for Collider Phenomenology,” *Comput. Phys. Commun.* **184**, 222 (2013) doi:10.1016/j.cpc.2012.09.009 [arXiv:1206.1599 [hep-ph]].
- [50] M. Cacciari and G. P. Salam, “Dispelling the N^3 myth for the k_t jet-finder,” *Phys. Lett. B* **641**, 57 (2006) doi:10.1016/j.physletb.2006.08.037 [hep-ph/0512210].
- [51] M. Cacciari, G. P. Salam and G. Soyez, “FastJet User Manual,” *Eur. Phys. J. C* **72**, 1896 (2012) doi:10.1140/epjc/s10052-012-1896-2 [arXiv:1111.6097 [hep-ph]].
- [52] M. Cacciari, G. P. Salam and G. Soyez, “The Anti- $k(t)$ jet clustering algorithm,” *JHEP* **0804**, 063 (2008) doi:10.1088/1126-6708/2008/04/063 [arXiv:0802.1189 [hep-ph]].
- [53] K. A. Olive *et al.* [Particle Data Group Collaboration], “Review of Particle Physics,” *Chin. Phys. C* **38**, 090001 (2014). doi:10.1088/1674-1137/38/9/090001
- [54] R. D. Ball *et al.* [NNPDF Collaboration], “Parton distributions for the LHC Run II,” *JHEP* **1504**, 040 (2015) doi:10.1007/JHEP04(2015)040 [arXiv:1410.8849 [hep-ph]].
- [55] A. Buckley, J. Ferrando, S. Lloyd, K. Nordstrm, B. Page, M. Rfenacht, M. Schnherr and G. Watt, “LHAPDF6: parton density access in the LHC precision era,” *Eur. Phys. J. C* **75**, 132 (2015) doi:10.1140/epjc/s10052-015-3318-8 [arXiv:1412.7420 [hep-ph]].
- [56] P. Artoisenet, R. Frederix, O. Mattelaer and R. Rietkerk, “Automatic spin-entangled decays of heavy resonances in Monte Carlo simulations,” *JHEP* **1303**, 015 (2013) doi:10.1007/JHEP03(2013)015 [arXiv:1212.3460 [hep-ph]].
- [57] F. Feruglio, L. Maiani and A. Masiero, “Right-handed Vector Bosons in $p\bar{p}$ and pp Collisions as a Source of Anomalous Events,” *Phys. Lett. B* **233**, 512 (1989). doi:10.1016/0370-2693(89)91350-6
- [58] T. G. Rizzo, “ Z' phenomenology and the LHC,” hep-ph/0610104.
- [59] F. M. L. Almeida, Jr., Y. do Amaral Coutinho, J. A. Martins Simoes, J. Ponciano, A. J. Ramalho, S. Wolck and M. A. B. Vale, “Minimal left-right symmetric models and new Z' properties at future electron-positron colliders,” *Eur. Phys. J. C* **38**, 115 (2004) doi:10.1140/epjc/s2004-02028-7 [hep-ph/0405020].
- [60] Z. Sullivan, “Fully differential W' production and decay at next-to-leading order in QCD,” *Phys. Rev. D* **66**, 075011 (2002) doi:10.1103/PhysRevD.66.075011 [hep-ph/0207290].
- [61] R. Gavin, Y. Li, F. Petriello and S. Quackenbush, “W Physics at the LHC with FEWZ 2.1,” *Comput. Phys. Commun.* **184**, 208 (2013) doi:10.1016/j.cpc.2012.09.005 [arXiv:1201.5896 [hep-ph]].

- [62] T. Jezo, M. Klasen, D. R. Lamprea, F. Lyonnet and I. Schienbein, “NLO+NLL limits on W' and Z' gauge boson masses in general extensions of the Standard Model,” JHEP **1412**, 092 (2014) doi:10.1007/JHEP12(2014)092 [arXiv:1410.4692 [hep-ph]].
- [63] F. Maltoni, G. Ridolfi and M. Ubiali, “b-initiated processes at the LHC: a reappraisal,” JHEP **1207**, 022 (2012) Erratum: [JHEP **1304**, 095 (2013)] doi:10.1007/JHEP04(2013)095, 10.1007/JHEP07(2012)022 [arXiv:1203.6393 [hep-ph]].
- [64] S. Dawson, A. Ismail and I. Low, “Redux on When is the top quark a parton?,” Phys. Rev. D **90**, no. 1, 014005 (2014) doi:10.1103/PhysRevD.90.014005 [arXiv:1405.6211 [hep-ph]].
- [65] T. Han, J. Sayre and S. Westhoff, “Top-Quark Initiated Processes at High-Energy Hadron Colliders,” JHEP **1504**, 145 (2015) doi:10.1007/JHEP04(2015)145 [arXiv:1411.2588 [hep-ph]].
- [66] M. Lim, F. Maltoni, G. Ridolfi and M. Ubiali, “Anatomy of double heavy-quark initiated processes,” JHEP **1609**, 132 (2016) doi:10.1007/JHEP09(2016)132 [arXiv:1605.09411 [hep-ph]].
- [67] J. C. Collins, D. E. Soper and G. F. Sterman, “Transverse Momentum Distribution in Drell-Yan Pair and W and Z Boson Production,” Nucl. Phys. B **250**, 199 (1985). doi:10.1016/0550-3213(85)90479-1
- [68] C. Degrande, O. Mattelaer, R. Ruiz and J. Turner, “Fully-Automated Precision Predictions for Heavy Neutrino Production Mechanisms at Hadron Colliders,” Phys. Rev. D **94**, no. 5, 053002 (2016) doi:10.1103/PhysRevD.94.053002 [arXiv:1602.06957 [hep-ph]].
- [69] C. Blaksley, M. Blennow, F. Bonnet, P. Coloma and E. Fernandez-Martinez, “Heavy Neutrinos and Lepton Number Violation in lp Colliders,” Nucl. Phys. B **852**, 353 (2011) doi:10.1016/j.nuclphysb.2011.06.021 [arXiv:1105.0308 [hep-ph]].
- [70] L. Duarte, G. A. Gonzalez-Sprinberg and O. A. Sampayo, “Majorana neutrinos production at LHeC in an effective approach,” Phys. Rev. D **91**, no. 5, 053007 (2015) doi:10.1103/PhysRevD.91.053007 [arXiv:1412.1433 [hep-ph]].
- [71] S. Mondal and S. K. Rai, “Polarized window for left-right symmetry and a right-handed neutrino at the Large Hadron-Electron Collider,” Phys. Rev. D **93**, no. 1, 011702 (2016) doi:10.1103/PhysRevD.93.011702 [arXiv:1510.08632 [hep-ph]].
- [72] M. Lindner, F. S. Queiroz, W. Rodejohann and C. E. Yaguna, “Left-Right Symmetry and Lepton Number Violation at the Large Hadron Electron Collider,” JHEP **1606**, 140 (2016) doi:10.1007/JHEP06(2016)140 [arXiv:1604.08596 [hep-ph]].
- [73] M. Cacciari, F. A. Dreyer, A. Karlberg, G. P. Salam and G. Zanderighi, “Fully Differential Vector-Boson-Fusion Higgs Production at Next-to-Next-to-Leading Order,” Phys. Rev. Lett. **115**, no. 8, 082002 (2015) doi:10.1103/PhysRevLett.115.082002 [arXiv:1506.02660 [hep-ph]].
- [74] C. Degrande, K. Hartling, H. E. Logan, A. D. Peterson and M. Zaro, “Automatic predictions in the Georgi-Machacek model at next-to-leading order accuracy,” Phys. Rev. D **93**, no. 3, 035004 (2016) doi:10.1103/PhysRevD.93.035004 [arXiv:1512.01243 [hep-ph]].
- [75] E. C. Aschenauer *et al.*, “eRHIC Design Study: An Electron-Ion Collider at BNL,” arXiv:1409.1633 [physics.acc-ph].

- [76] CMS Collaboration [CMS Collaboration], “Search for SSM W’ production, in the lepton+MET final state at a center-of-mass energy of 13 TeV,” CMS-PAS-EXO-15-006.
- [77] Y. L. Dokshitzer, G. D. Leder, S. Moretti and B. R. Webber, “Better jet clustering algorithms,” JHEP **9708**, 001 (1997) doi:10.1088/1126-6708/1997/08/001 [hep-ph/9707323].
- [78] M. Wobisch and T. Wengler, “Hadronization corrections to jet cross-sections in deep inelastic scattering,” In *Hamburg 1998/1999, Monte Carlo generators for HERA physics* 270-279 [hep-ph/9907280].
- [79] The ATLAS collaboration [ATLAS Collaboration], “Search for new resonances decaying to a charged lepton and a neutrino in pp collisions at $\sqrt{s} = 13$ TeV with the ATLAS detector,” ATLAS-CONF-2016-061.
- [80] P. Z. Skands and D. Wicke, “Non-perturbative QCD effects and the top mass at the Tevatron,” Eur. Phys. J. C **52**, 133 (2007) doi:10.1140/epjc/s10052-007-0352-1 [hep-ph/0703081 [HEP-PH]].
- [81] A. H. Hoang and I. W. Stewart, “Top Mass Measurements from Jets and the Tevatron Top-Quark Mass,” Nucl. Phys. Proc. Suppl. **185**, 220 (2008) doi:10.1016/j.nuclphysbps.2008.10.028 [arXiv:0808.0222 [hep-ph]].
- [82] G. Aad *et al.* [ATLAS Collaboration], “Determination of the top-quark pole mass using $t\bar{t} + 1$ -jet events collected with the ATLAS experiment in 7 TeV pp collisions,” JHEP **1510**, 121 (2015) doi:10.1007/JHEP10(2015)121 [arXiv:1507.01769 [hep-ex]].
- [83] M. Dasgupta and G. P. Salam, “Resummation of nonglobal QCD observables,” Phys. Lett. B **512**, 323 (2001) doi:10.1016/S0370-2693(01)00725-0 [hep-ph/0104277].
- [84] A. Banfi, G. Corcella and M. Dasgupta, “Angular ordering and parton showers for non-global QCD observables,” JHEP **0703**, 050 (2007) doi:10.1088/1126-6708/2007/03/050 [hep-ph/0612282].
- [85] A. Banfi, M. Dasgupta, K. Khelifa-Kerfa and S. Marzani, “Non-global logarithms and jet algorithms in high-pT jet shapes,” JHEP **1008**, 064 (2010) doi:10.1007/JHEP08(2010)064 [arXiv:1004.3483 [hep-ph]].
- [86] N. Fischer, S. Gieseke, S. Pltzer and P. Skands, “Revisiting radiation patterns in e^+e^- collisions,” Eur. Phys. J. C **74**, no. 4, 2831 (2014) doi:10.1140/epjc/s10052-014-2831-5 [arXiv:1402.3186 [hep-ph]].